

# Wetting and Prewetting Phase Transitions facilitated by Surface Binding

Xueping Zhao,<sup>1,2</sup> Giacomo Bartolucci,<sup>1,2</sup> Alf Honigmann,<sup>3,2</sup>

Frank Jülicher,<sup>1,2,4</sup> and Christoph A. Weber<sup>a1,2</sup>

<sup>1</sup>*Max Planck Institute for the Physics of Complex Systems,  
Nöthnitzer Strasse 38, 01187 Dresden, Germany*

<sup>2</sup>*Center for Systems Biology Dresden,  
Pfotenhauerstrasse 108, 01307 Dresden, Germany*

<sup>3</sup>*Max Planck Institute of Molecular Cell Biology and Genetics,  
Pfotenhauerstrasse 108, 01307 Dresden, Germany*

<sup>4</sup>*Cluster of Excellence Physics of Life,  
TU Dresden, 01062 Dresden, Germany*

(Dated: July 5, 2021)

## Abstract

In living cells, protein-rich condensates can wet the cell membrane and surfaces of membrane-bound organelles. Interestingly, many phase-separating proteins also bind to membranes leading to a molecular layer of bound molecules. Here we investigate how binding to membranes affects surface phase transitions such as wetting and prewetting. We derive a thermodynamic theory for a three-dimensional bulk in the presence of a two-dimensional, flat membrane. Above the saturation concentration, we find that membrane binding facilitates complete wetting and lowers the wetting angle. Moreover, below the saturation concentration, binding facilitates the formation of a thick layer at the membrane and thereby shifts the prewetting phase transition far below the saturation concentration. The distinction between bound and unbound molecules near the surface leads to a large variety of prewetted states. Our work suggests that surface phase transitions combined with molecular binding represent a versatile mechanism to control the formation of protein-rich domains at intra-cellular surfaces.

---

<sup>a</sup> Corresponding author: weber@pks.mpg.de

## I. INTRODUCTION

Surfaces introduce a new level of complexity, as Wolfgang Pauli alluded to in his famous quote: “God made the bulk; surfaces were invented by the devil” [1]. Surfaces are ubiquitous in nature and key determinants in many complex systems. A paradigm are living cells which are surrounded by a membrane and contain intricate organelles enclosed by membranes. While a major function of membranes is to compartmentalize biochemical reactions in cells, the interplay between membranes and the cellular bulk is crucial for many biological processes. Examples are sensing and signalling, endocytosis or asymmetric cell division. In addition to membranes, cells use protein-rich condensates to organize cellular space. Such condensates coexist with the cellular surrounding and share hallmark properties of physical droplets [2–6]. Interestingly, protein condensates can adhere to intracellular surfaces and membrane-bound organelles [2, 7, 8], which resemble condensates wetted on surfaces. These observations indicate that phase-separating proteins in living cells not only phase-separate in the bulk but can also undergo surface phase transitions.

The theory of surface phase transitions was developed by Cahn [9]. In this seminal work, he discussed the graphical construction for wetting transitions but also showed the existence of prewetting transitions. The wetting transition separates the regime of complete wetting and partial wetting, where the interface of wetting droplets exhibits a contact angle with respect to the surface [9–17]. While wetting solely occurs inside the binodal of the corresponding bulk phase diagram (supersaturated regime), prewetting phase transitions take place in the undersaturated regime where droplets shrink and disappear in the bulk. Inside the prewetting regime of the phase diagram, a three-dimensional layer forms close to the surface which we refer to as the “thick layer”. The layer thickness can be quantified by the excess surface concentration which serves as an order parameter for the wetting and prewetting transitions. Crossing the prewetting transition, e.g. by lowering the bulk concentration, the excess surface concentration (order parameter) decreases discontinuously to a lower value and molecules accumulate only very weakly at the surface, forming the “thin layer”. The close vicinity of the prewetting transition line and the binodal for many polymeric systems was an experimental challenge to distinguish bulk and surface transitions [18–20].

Interestingly, many of the phase-separating proteins have molecular domains by which they can bind to membranes [21–23]. Reversible membrane binding of proteins in the presence of chemical feedback is known to give rise to reaction-diffusion patterns on membranes [24–26]. In contrast to wetted or prewetted states, these patterns are comprised of mono-layered, two-dimensional domains of specific protein composition leading to a spatially organized membrane. Wetting or prewetting

can however give rise to surface condensates that are three-dimensional. Such condensates can serve as hubs for down-stream assembly processes at membrane surfaces [23, 27, 28]. Prewetting could also serve as a mechanism for the formation of proteins condensates on DNA strands [29, 30] and thus play a role in chromatin organization. In summary, condensation at surfaces such as membranes or biofilaments appears as a key principle of spatial organization of biological surfaces [31]. However, a general thermodynamic theory that explores how protein binding to biological surfaces affects surface condensation is lacking.

In this work, we study surface phase transitions such as wetting and prewetting for systems where molecules bind to a surface. We propose a general thermodynamic free energy that captures the molecular interactions in the three-dimensional bulk and a two-dimensional, flat membrane surface. Using this free energy, we determine the phase diagram for wetting and prewetting at thermodynamic equilibrium. We find that varying parameters that describe surface binding of molecules leads to phase diagrams of variable complexity and topology that exhibit transitions between a rich set of thermodynamic surface states (Fig. 8). A key finding is that binding can enlarge the prewetting regime and move the prewetting transition to lower bulk concentrations.

## II. THERMODYNAMICS OF PHASE SEPARATION WITH MEMBRANE BINDING

We consider a liquid solution where solute molecules can bind to specific sites on a two-dimensional, flat membrane at  $z = 0$ . The volume fraction of molecules in the bulk is denoted by  $\phi(x, y, z)$ , the density of molecules bound to the membrane is described by the area fraction  $\phi_m(x, y)$ . During binding and unbinding events molecules transition between the solute state and the surface bound state according to

$$\phi \rightleftharpoons \phi_m. \quad (1)$$

In this system we study the physics of condensation and how wetting and prewetting phenomena are influenced by membrane binding (Fig. 1a-c). To this end, we consider a bulk binary mixture of volume  $V$  which is composed of solute molecules and solvent. The free energy contains contributions from the bulk  $f_b(\phi)$ , the membrane  $f_m(\phi_m)$  and coupling free energy between them,  $J(\phi|_0, \phi_m)$ :

$$F[\phi, \phi_m] = \int_V d^3x \left[ f_b(\phi) + \frac{1}{2} \kappa |\nabla \phi|^2 \right] + \int_m d^2x \left[ f_m(\phi_m) + \frac{1}{2} \kappa_m |\nabla_{\parallel} \phi_m|^2 + J(\phi|_0, \phi_m) \right], \quad (2)$$

where  $\phi|_0$  is the bulk volume fraction at the membrane surface. Moreover,  $\kappa$  and  $\kappa_m$  characterize the corresponding free energy penalties for gradients in bulk and membrane, respectively, and

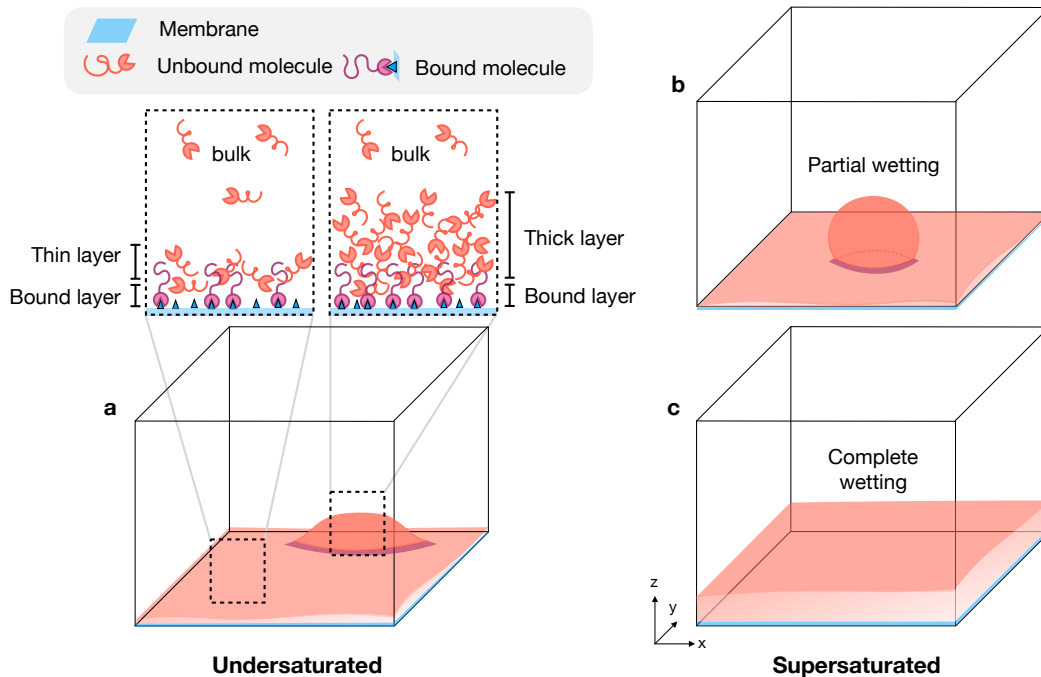


FIG. 1. **Schematics of surface phase transitions in the presence of membrane binding.** Molecules from the bulk can bind to specific sites (blue triangles) on the membrane (blue surface). Unbound bulk molecules can also accumulate adjacent to the membrane surface, leading to the formation of three dimensional layers on the membrane surface (red surfaces). **(a)** If the system is undersaturated ( $\phi_\infty < \phi_{\text{out}}^{\text{eq}}$ ), prewetted thin and thick layers can transiently form. At thermodynamic equilibrium, either thin or thick layers are stable except at the prewetting transition where both states coexist. For supersaturated conditions, condensates either partially wet **(b)** or completely wet the membrane surface **(c)**, depending on the molecular interactions and the interactions with the surface.

$\nabla_{\parallel} = (\partial_x, \partial_y)$  denotes the gradient vector in the membrane plane. From Eq. (2) we can define the local chemical potential  $\mu = \nu_b \delta F / \delta \phi$  and  $\mu_m = \nu_m \delta F / \delta \phi_m$ , where  $\nu_b$  and  $\nu_m$  denote the molecular volume and the molecular surface area of the molecules, respectively.

### A. Thermodynamics of a semi-infinite system

We consider a semi-infinite, thermodynamic system with the membrane at  $z = 0$ . Systems that are homogeneous in the  $x$ - $y$  plane become effectively one-dimensional with a bulk volume fraction  $\phi(z)$  changing along the  $z$ -direction with  $z \in [0, \infty)$ . The corresponding Helmholtz surface free

energy functional reads

$$f_s[\phi, \phi_m] = \int_0^\infty dz \left[ f_b(\phi) - f_b(\phi_\infty) + \frac{1}{2} \kappa |\partial_z \phi|^2 \right] + f_m(\phi_m) + J(\phi|_0, \phi_m), \quad (3)$$

where  $\phi_\infty = \phi(z \rightarrow \infty)$  with the corresponding the external chemical potential  $\mu_\infty = df_b/d\phi|_{\phi=\phi_\infty}$ .

We also define the excess surface concentration

$$c_s = \int_0^\infty dz \left[ \frac{1}{\nu_b} (\phi(z) - \phi_\infty) \right]. \quad (4)$$

Evaluating  $f_s$  for the profile  $\phi(z)$  that minimizes Eq. (3) for fixed  $c_s$  and  $\phi_m$  with  $\phi_\infty$  given far away from the membrane gives the surface free energy  $f_s(c_s, \phi_m)$  with units of an energy per area. It depends on the membrane area fraction  $\phi_m$  and the excess surface concentration  $c_s$ . The chemical potentials in bulk and membrane can now be expressed as

$$\mu = \frac{\partial f_s}{\partial c_s}, \quad (5a)$$

$$\mu_m = \nu_m \frac{\partial f_s}{\partial \phi_m}. \quad (5b)$$

We can use a Legendre transformation to define the Gibbs surface free energy which is the surface thermodynamic potential in the ensemble where the chemical potentials are fixed:

$$\gamma_s(\mu, \mu_m) = f_s(c_s, \phi_m) - \mu c_s - \mu_m \frac{\phi_m}{\nu_m}. \quad (6)$$

The conjugate variables to each of the chemical potentials  $\mu$  and  $\mu_m$  are the excess surface concentration  $c_s$  and the area fraction  $\phi_m$ ,

$$c_s = -\frac{\partial \gamma_s}{\partial \mu}, \quad (7a)$$

$$\phi_m = -\nu_m \frac{\partial \gamma_s}{\partial \mu_m}. \quad (7b)$$

## B. Free energy minimization in a semi-infinite system

We determine the equilibrium states via minimization of the Helmholtz surface free energy functional  $f_s[\phi, \phi_m]$ , while keeping  $c_s$  and  $\phi_m$  fixed. This is achieved by minimizing the the Gibbs surface free energy functional  $\gamma_s[\phi, \phi_m] = f_s[\phi, \phi_m] - \mu c_s - \mu_m \frac{\phi_m}{\nu_m}$ , where  $\mu$  and  $\mu_m$  act as Lagrange multipliers to impose fixed  $c_s$  and  $\phi_m$ . At this minimum,  $\delta \gamma_s = 0$ , where

$$\begin{aligned} \delta \gamma_s[\phi, \phi_m] = & \int_0^\infty dz \left[ \left( \frac{\partial f_b}{\partial \phi} - \frac{1}{\nu_b} \mu - \kappa \partial_z^2 \phi \right) \delta \phi \right] + \kappa \frac{d\phi}{dz} \delta \phi \Big|_0^\infty \\ & + \left[ \frac{\partial f_m}{\partial \phi_m} + \frac{\partial J(\phi|_0, \phi_m)}{\partial \phi_m} - \frac{1}{\nu_m} \mu_m \right] \delta \phi_m + \frac{\partial J(\phi|_0, \phi_m)}{\partial \phi|_0} \delta \phi \Big|_0 \end{aligned} \quad (8)$$

is the functional variation of the Gibbs free energy functional  $\gamma_s[\phi, \phi_m]$ . This leads to the equilibrium conditions:

$$\frac{\partial f_b}{\partial \phi} - \frac{1}{\nu_b} \mu_\infty - \kappa \partial_z^2 \phi = 0, \quad z \in [0, \infty), \quad (9a)$$

$$\kappa \frac{d\phi}{dz} \Big|_{z=\infty} = 0, \quad (9b)$$

$$-\kappa \frac{d\phi}{dz} \Big|_{z=0} + \frac{\partial J(\phi, \phi_m)}{\partial \phi} \Big|_{z=0} = 0, \quad (9c)$$

$$\frac{\partial f_m}{\partial \phi_m} + \frac{\partial J(\phi, \phi_m)}{\partial \phi_m} \Big|_{z=0} - \frac{1}{\nu_m} \mu_\infty = 0, \quad (9d)$$

where we used that binding between membrane and bulk (Eq. (1)) is at thermodynamic equilibrium:  $\mu_m = \mu_\infty$ , where  $\mu_\infty$  denotes the chemical potential of the reservoir. By integration over the bulk (see Appendix A) and using Eq. (9b), we can rewrite Eqs. (9),

$$\partial_z \phi \pm \sqrt{\frac{2}{\kappa} W(\phi)} = 0, \quad z \in [0, \infty), \quad (10a)$$

$$\sqrt{2\kappa W(\phi|_0)} \pm \frac{\partial J(\phi, \phi_m)}{\partial \phi} \Big|_0 = 0, \quad (10b)$$

$$\frac{\partial f_m}{\partial \phi_m} + \frac{\partial J(\phi, \phi_m)}{\partial \phi_m} \Big|_{z=0} - \frac{1}{\nu_m} \mu_\infty = 0, \quad (10c)$$

where  $W(\phi) V$  is the free energy needed to create a uniform fluid volume  $V$  of composition  $\phi$  from the reservoir of composition  $\phi_\infty$  [9],

$$W(\phi) = f_b(\phi) - \mu_\infty \frac{1}{\nu_b} \phi + \Pi_\infty, \quad (10d)$$

and  $\Pi_\infty = -f_b(\phi_\infty) + \mu_\infty \frac{1}{\nu_b} \phi_\infty$  is the osmotic pressure of the particle bath at  $z \rightarrow \infty$ . Note that  $\pm$  indicates that we need to solve Eq. (10a) and Eq. (10b) with both signs to obtain all solutions of Eq. (9) (for details see Appendix A).

We use Eqs. (10b) and (10c) to obtain the membrane area fraction  $\phi_m$  and bulk volume fraction at the surface  $\phi|_0$ . The spatial bulk profile  $\phi(z)$  then follows from Eq. (10a). Using this profile we can compute the excess surface concentration  $c_s$  (Eq. (4)). The thermodynamic control parameter is the chemical potential of the reservoir,  $\mu_\infty$ . We also use the volume fraction of the reservoir  $\phi_\infty$  as control parameter, which is equivalent to the average volume fraction  $\bar{\phi}$  in the thermodynamic limit. We calculate the surface phase diagrams as a function of  $\bar{\phi}$  and parameters characterising the interactions among the molecules (see Sect. (III A)).

### C. Surface phase diagrams obtained via graphical construction

The transition lines separating different thermodynamic states at the surface can also be obtained via a graphical construction. Using Eqs. (10a), we can rewrite the Gibbs surface free energy functional (Eq. (6) with  $f_s$  given by Eq. (3)) leading to

$$\gamma(\phi, \phi_\infty) = \int_{\phi_\infty}^{\phi} d\phi' \left[ \pm \sqrt{2\kappa W(\phi')} + \frac{\partial \hat{J}}{\partial \phi'} \right] + \hat{J}(\phi_\infty, \phi_m), \quad (11)$$

where  $\hat{J}(\phi, \phi_m) = J(\phi, \phi_m) + f_m(\phi_m) - \nu_m^{-1} \mu_\infty \phi_m$ , with  $\partial \hat{J} / \partial \phi_m = 0$  (see Eq. (10c)), and  $\phi|_0$  and  $\phi_m$  are determined by Eq. (10b). The integral term in Eq. (11) corresponds to the area between  $\pm \sqrt{2\kappa W(\phi)}$  and  $-\frac{\partial \hat{J}}{\partial \phi}$  and can be illustrated graphically (see colored areas in Fig. 2).

Now we can define the Gibbs surface potential as  $\gamma_s = \gamma(\phi|_0, \phi_\infty)$ . Local extrema of the Gibbs surface potential correspond to the intersection points between  $\pm \sqrt{2\kappa W(\phi)}$  and  $-\frac{\partial \hat{J}}{\partial \phi}$ . There can be two local minima,  $\gamma_\alpha = \gamma_s(\phi|_{0,\alpha}, \phi_\infty)$  and  $\gamma_\beta = \gamma_s(\phi|_{0,\beta}, \phi_\infty)$ , and the intermediate local maximum is denoted by  $\gamma_u = \gamma_s(\phi|_{0,u}, \phi_\infty)$ . The differences between these extremal values of the Gibbs surface potential can be expressed as the areas between  $\pm \sqrt{2\kappa W(\phi)}$  and  $-\frac{\partial \hat{J}}{\partial \phi}$ . Specifically,  $\gamma_\alpha = -S_0 + \hat{J}(\phi_\infty, \phi_m)$ ,  $\gamma_u = -S_0 + S_1 + \hat{J}(\phi_\infty, \phi_m)$  and  $\gamma_\beta = -S_0 + S_1 - S_2 + \hat{J}(\phi_\infty, \phi_m)$  (see colored domains in Fig. 2(a.1,b.1)). Thus, we find that the surface free energies at the minima are related by

$$\gamma_\alpha = \gamma_\beta + S_1 - S_2. \quad (12)$$

At the prewetting and wetting transition lines, the Gibbs surface free energies of both states  $\alpha$  and  $\beta$  are equal:

$$\gamma_\alpha = \gamma_\beta, \quad (13)$$

which implies, using Eq. (12), that  $S_1 = S_2$  at the transition line. This defines the graphical construction and determines the value of the control parameter, e.g.  $\bar{\phi}$ , at which the transition occurs. The minimized surface free energies exhibit a kink at the wetting and prewetting transition. Thus, the two order parameters, area fraction  $\phi_m$  and the excess surface concentration  $c_s$ , change discontinuously at the surface phase transition.

If the system is supersaturated, the average volume fraction  $\bar{\phi}$  obeys  $\bar{\phi} > \phi_\alpha$  and the bulk volume fraction could either take the equilibrium values  $\phi_\alpha$  and  $\phi_\beta$ . Based on the definition of Gibbs surface free energy density  $\gamma_s = \gamma(\phi|_0, \phi_\infty)$  given in Eq. (11), we identify the surface tensions between the membrane and the dilute phase ( $\phi_\infty = \phi_\alpha$ ), the membrane and the dense phase ( $\phi_\infty = \phi_\beta$ ), and

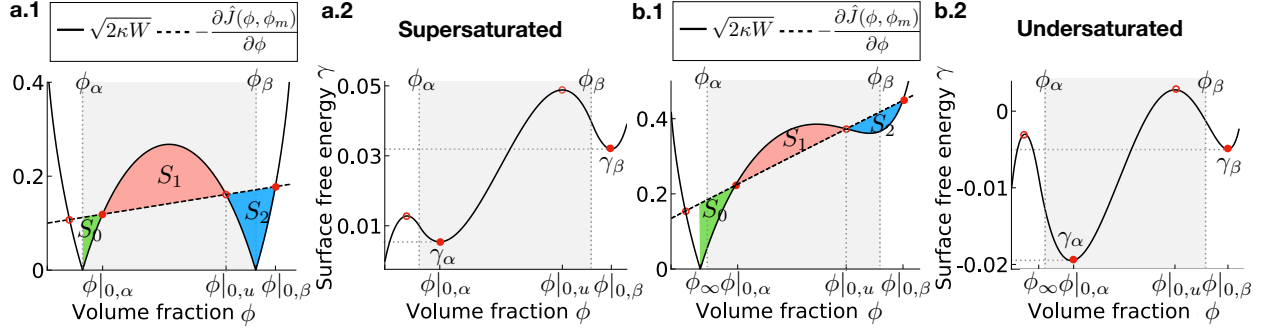


FIG. 2. **Graphical construction for wetting and prewetting with membrane binding.** To obtain the equilibrium state at which the surface free energy  $\gamma_s$  is minimal, we perform a graphical construction by comparing  $\sqrt{2\kappa W}$  (solid line) and  $-\partial\hat{J}(\phi, \phi_m)/\partial\phi$  (dashed line) for wetting (**a.1**) and prewetting (**b.1**), respectively. The intersections of both functions can give two unstable solutions (open red circles) and two locally stable solutions (red dots). The locally stable solution that has the lower Gibbs surface free energy  $\gamma_s$  corresponds to the thermodynamic equilibrium state; see (**a.2**) for wetting and (**b.2**) for the case of prewetting. At a surface phase transition, the Gibbs surface free energies  $\gamma_\alpha = \gamma(\phi|_{0,\alpha}, \phi_\infty)$  and  $\gamma_\beta = \gamma_s(\phi|_{0,\beta}, \phi_\infty)$  are equal (Eq. (13)), which amounts to  $S_1 = S_2$  (Eq. (12)). The gray shaded area represents the demixed regime (supersaturated) where the bulk can phase separate into a dilute phase ( $\phi_\alpha$ ) and a dense phase ( $\phi_\beta$ ). Here, we only illustrate the branch  $\sqrt{2\kappa W}$ ; see Fig. 9 for the graphic construction with both branches  $\pm\sqrt{2\kappa W}$ .

between the dilute and dense phase:

$$\gamma_{s,\alpha} = \gamma(\phi|_{0,\alpha}, \phi_\alpha), \quad (14a)$$

$$\gamma_{s,\beta} = \gamma(\phi|_{0,\beta}, \phi_\beta), \quad (14b)$$

$$\gamma_{\alpha,\beta} = \int_{\phi_\alpha}^{\phi_\beta} d\phi \sqrt{2\kappa W}. \quad (14c)$$

These equations satisfy the Young–Dupré law,  $\gamma_{s,\alpha} = \gamma_{s,\beta} + \gamma_{\alpha,\beta} \cos(\theta)$ , which defines the contact angle. The wetting transition is characterized by equal Gibbs surface free energy of the partially wetted state  $\gamma_\alpha = \gamma_{s,\alpha}$ , and the completely wetted state  $\gamma_\beta = \gamma_{s,\beta} + \gamma_{\alpha,\beta}$  (Eq. (13)), corresponding to zero contact angle,  $\theta = 0$ .

If the system is undersaturated ( $\bar{\phi} < \phi_\alpha$ ), there can still be two states corresponding two local minima of the Gibbs surface free energy as can be seen from the graphical construction Eq. (12). The prewetting transition occurs when Eq. (13) is satisfied and these free energies are equal.



#### D. Bulk and membrane free energies

To calculate the surface phase diagram using the graphical construction as well as the profile  $\phi(z)$  at thermodynamic equilibrium, we consider the following free energy for the bulk ( $b$ ) and membrane ( $m$ ):

$$f_b(\phi) = \frac{k_B T}{\nu} \left[ \frac{1}{n_b} \phi \ln \phi + (1 - \phi) \ln(1 - \phi) + \chi_b \phi (1 - \phi) \right], \quad (15a)$$

$$f_m(\phi_m) = \frac{k_B T}{\tilde{\nu}} \left[ \frac{1}{n_m} \phi_m \ln \phi_m + (1 - \phi_m) \ln(1 - \phi_m) + \chi_m \phi_m (1 - \phi_m) + \omega_m \phi_m \right], \quad (15b)$$

where  $\nu$  and  $\tilde{\nu}$  are the solvent molecular volume and solvent molecular surface area, respectively. Bulk molecules have a molecular volume of  $\nu_b = \nu n_b$ , while bound molecules occupy an area of  $\nu_m = \tilde{\nu} n_m$ . Here,  $n_b$  and  $n_m$  are the fractions of molecular volumes or surface areas of the molecules compared to the solvent, respectively. Molecular interactions in the bulk and membrane are governed by the interaction parameters  $\chi_b$  and  $\chi_m$ . Both parameters are in general different since interactions can change upon binding. The internal free energies difference between membrane molecules and bulk molecules is denoted by  $\omega_m$ .

The coupling free energy between bulk and membrane reads

$$J(\phi, \phi_m) = \frac{k_B T}{\tilde{\nu}} \left[ \omega_b \phi + \chi_{bb} \phi^2 + \chi_{bm} \phi \phi_m \right], \quad (15c)$$

where  $\chi_{bm}$  characterizes the interactions between membrane-bound molecules and bulk molecules at the surface. Moreover,  $\omega_b$  is the internal free energy of a bulk molecule at the surface. When surfaces are attractive for molecules in the bulk,  $\omega_b < 0$ . The coefficient  $\chi_{bb}$  accounts for interactions of bulk molecules accumulating at the surfaces.

### III. EFFECTS OF MEMBRANE BINDING ON SURFACE PHASE TRANSITIONS

#### A. Wetting and prewetting without phase separation in the membrane

Here we first study how binding affects wetting and prewetting for cases where the surface free energy  $f_s$  of membrane alone cannot give rise to coexisting phases ( $\chi_m = -4$ ). For simplicity, we set the membrane insertion energy  $\omega_m$  to zero. We choose  $\omega_b = -0.3$  and  $\chi_{bb} = 0$  for the coupling parameters between surface and bulk. We study the effects of binding as a function of the bulk interaction parameter  $\chi_b$ , the bulk volume fraction  $\phi_\infty$ , and the coupling parameter between bulk and membrane  $\chi_{bm}$ . As a reference, we consider the same system in the absence of membrane binding,  $\chi_{bm} = 0$ . Please note that the transition line for our model without binding,  $\phi_m = 0$ ,

is the same as in the case with binding and vanishing bulk-membrane coupling ( $\chi_{bm} = 0$ ). The corresponding surface phase diagram is shown in Fig. 3a. This diagram depicts the domains with partially and completely wetted states separated by the wetting transition (blue line). It also shows the prewetting line (green line) separating thin and thick layer states. At both transitions, the excess surface concentration  $c_s$  is discontinuous. The red star represents the prewetting critical point where thin and thick layer state become indistinguishable.

*1. Membrane binding favors complete wetting and reduces the contact angle*

Binding to the membrane has significant effects on the wetting transition (compare Fig. 3a and 3b). In particular, when increasing the attraction between the bulk and the membrane by reducing  $\chi_{bm}$ , complete wetting is favored. This trend is evident in an upshift of the bulk interaction parameter at which the wetting transition occurs,  $\chi_b^*$ , with decreasing coupling parameter  $\chi_{bm}$  (blue line in Fig. 3(c)). Please note that at the wetting transition, there is a kink in the surface free energies (Eq. (13)) and the excess surface concentration  $c_s$  and membrane area fraction  $\phi_m$  jumps. In addition, for more attractive couplings between membrane and bulk, the wetting angle decreases (colored lines in Fig. 3(d)). This behavior is not only due to the shift of the wetting transition  $\chi_b^*(\chi_{bm})$ . Since the coupling is a second order term that describes the interactions between membrane and bulk, the trend of decreasing wetting angle with more attractive  $\chi_{bm}$  persists even after recaling  $\chi_b$  by the wetting transition  $\chi_{bm}^*$ .

*2. Prewetting transition shifts to lower concentrations*

Membrane binding not only affects the wetting transition line  $\chi_b^*(\chi_{bm})$  but also changes the prewetting transition line (compare green line in Fig. 3(a) with (b)). These changes result from the fact that at the prewetting line not only  $c_s$  but also the area fraction of bound molecules  $\phi_m$  is in general discontinuous (Fig. (4)). In particular, since the prewetting line is linked to the wetting transition at the dilute branch of the binodal, the upshift of the wetting line for more attractive coupling also moves the prewetting line to smaller volume fractions  $\phi$ . In addition, the critical point (red star) changes in a non-linear fashion with the coupling strength (Fig. 3(c)). Both trends significantly widen the prewetting regime (light red area), making the prewetting regime accessible for a broad range of interaction and coupling parameters. Interestingly, when the attractive coupling parameters is varied within a physically meaningful range in the order of a few

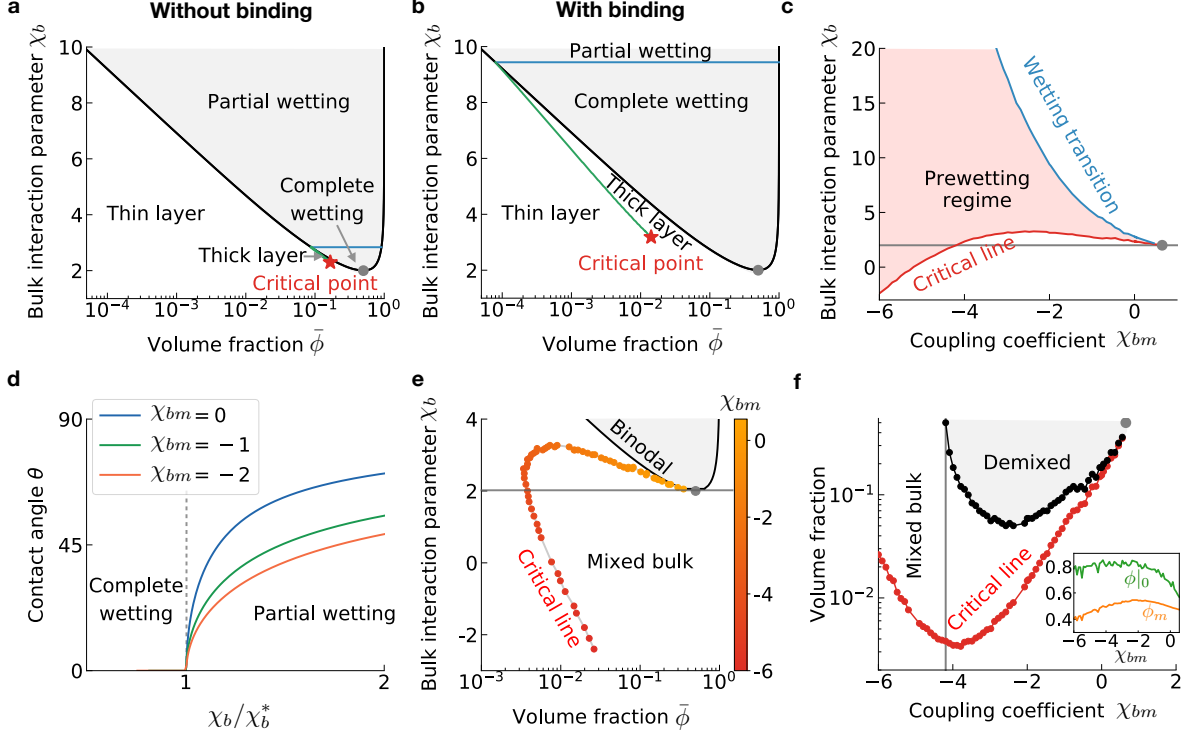


**FIG. 3. Membrane binding strongly affects the wetting and prewetting transition.** (a) Surface phase diagram without binding to membrane. Note that  $\chi_{bm} = 0$  leads to the same transition lines while heterogeneous states are different. (b) Surface phase diagram with binding and attractive coupling between membrane and bulk ( $\chi_{bm} = -2$ ) illustrating that binding can shift the wetting transition line  $\chi_b^*$  (blue) upwards and the prewetting transition line (green) far away from the binodal (black). The red star is the prewetting critical point and the gray dot the bulk critical point. (c) The prewetting regime (light red), enclosed by the wetting transition (blue) and the critical prewetting line (red), widens as the coupling  $\chi_{bm}$  gets more attractive. (d) Contact angle  $\theta$  of partially wetted condensates in the demixed phase as a function of the rescaled bulk interaction parameter  $\chi_b/\chi_b^*$  for three values of the bulk-membrane coupling,  $\chi_{bm} = 0, -1, -2$ . This indicates that  $\theta$  does not only change with  $\chi_{bm}$  due to the shift of the wetting line. (e, f) The prewetting critical line (shades of red) is shifted to strongly undersaturated regimes for more attractive bulk-membrane coupling  $\chi_{bm}$ . There is a minimal critical volume fraction since the critical  $\chi_b$  decreases for more attractive bulk-membrane coupling  $\chi_{bm}$ . Thus, molecules favor mixing with the bulk which is evident by a decrease of molecules adjacent and bound to the surface (see inset in (f)). Black dots in (f) represent the volume fractions of the binodal in (e) corresponding to the same  $\chi_b$  values as the critical prewetting point.

$k_B T$ , the volume fraction of the prewetting critical point can decrease by more than one order of magnitude (Fig. 3(e,f)). This implies that, due to binding, thick layers on the surface can already form via prewetting at bulk volume fraction far below the supersaturation level (compare red data

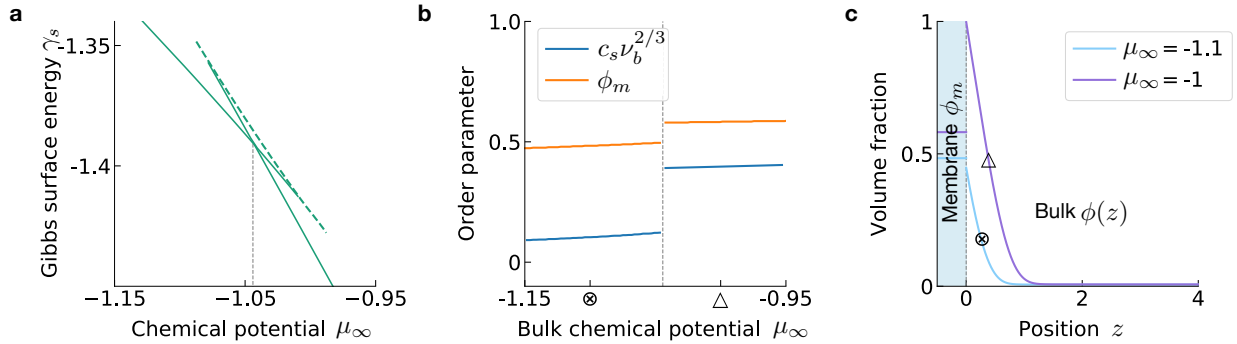


FIG. 4. **Characteristics of prewetting phase transitions with binding and no phase separation in the membrane.** (a) The Gibbs surface energy  $\gamma_s$  shows a kink at the prewetting phase transition ( $\chi_b = 4$  in Fig. 3b). (b) This kink implies a jump of both order parameters, the excess surface concentration  $c_s$  and the fraction of molecules bound at the membrane,  $\phi_m$ . (c) Depending on the amount of particles in the system characterized by the chemical potential  $\mu_\infty$ ,  $\phi_m$  and  $\phi|_0$  differ and thus the thickness of the bulk layers  $\phi(z)$  varies.

points to binodal indicated by black line). Surprisingly, there is a minimum of critical volume fraction of the prewetting transition (Fig. 3(e,f)). This minimum arises because the critical values of the bulk interaction parameter  $\chi_b$  also decrease for strongly attractive coupling strength  $\chi_{bm}$ . A decreased bulk interaction parameter corresponds to interactions among bulk molecules becoming less attractive or even repulsive, in turn disfavoring the presence of bulk molecules adjacent to the membrane (inset, Fig. (3)(f)). This also decreases the population of molecules bound to the surface  $\phi_m$  (inset). Therefore, we conclude that the minimal value of the critical prewetting volume fraction arises from a competition of the energy gain of molecules being bound and adjacent to the surface (favored for attractive coupling strength  $\chi_{bm}$ ) and the energy gain of molecules mixing with solvent in the bulk (favored by negative bulk interaction parameter  $\chi_b$  corresponding to attractive solvent-bulk interactions).

### 3. Prewetting transition persists below the bulk critical point

In the absence of membrane binding, prewetting transitions can only occur for bulk interaction parameters above the bulk critical point where bulk phase separation is possible (gray dots are below the red star in Fig. 3a). The attractive coupling between bulk and membrane enables situations where the prewetting critical point shifts to values of bulk interaction parameter below the bulk critical point, where the bulk cannot phase-separate for any volume fraction  $\phi$  (see domains

separated by gray line, entitled “Mixed bulk” in Fig. 3(e,f)). In other words, binding mediates prewetting that is robust against concentration perturbations and that controls the formation of three-dimensional thick layers at surfaces, while phase separation in the bulk is suppressed. Similar findings were recently reported in experimental studies of functionalized surfaces and confirmed by corresponding Brownian dynamic simulations [32].

## B. Wetting and prewetting with phase separation in the membrane

In this section, we will discuss how binding affects wetting and prewetting if molecules bound to the membrane can phase-separate which corresponds to a repulsive interaction parameter of bound molecules, which we chose  $\chi_m = 3$ . In all the following studies, we fix the coupling coefficients characterizing the interactions of bulk molecules with the surface,  $\omega_b = -0.3$  and  $\chi_{bb} = -0.5$ . We vary the average volume fractions  $\bar{\phi}$  and the bulk interaction parameter  $\chi_b$  to calculate the corresponding surface phase diagrams. We discuss two choices for the coupling strength between membrane and bulk: an attractive interaction parameter  $\chi_{bm} = -0.1$  and a repulsive one  $\chi_{bm} = 0.3$ , respectively. We find multiple striking effects on wetting and prewetting due to phase separation in membrane.

### 1. Prewetting transitions between four distinct surface states

When bound molecules can phase-separate in the membrane, wetting and prewetting transitions are affected due to the mutual coupling between membrane and bulk. This coupling is characterized by the coupling coefficient  $\chi_{bm}$ , which links the behavior of the two respective order parameters  $\phi_m$  and  $c_s$ . In general, we find that there are four types of thermodynamic states in the undersaturated regime ( $\bar{\phi} < \phi_\alpha$ ). These four surface states are the combinatoric possibilities between a thick or thin surface layer (high or low  $c_s \nu_b^{2/3}$ ), and a dense or dilute phase of membrane-bound molecules (high or low  $\phi_m$ ); see Fig. 5(a) and 6(a). Similar to the case without phase separation of bound molecules in the membrane (Fig. 3(c)), such new thermodynamic prewettted states can be found in a broad range of bulk volume fractions and bulk interaction parameters. Moreover, the transition lines separating such surface states intersect at triple points where three prewettted states can coexist.

The existence of multiple thermodynamic surface states can lead to complex Gibbs loops around the transition between two thermodynamic states. A classical Gibbs loop consists of two locally

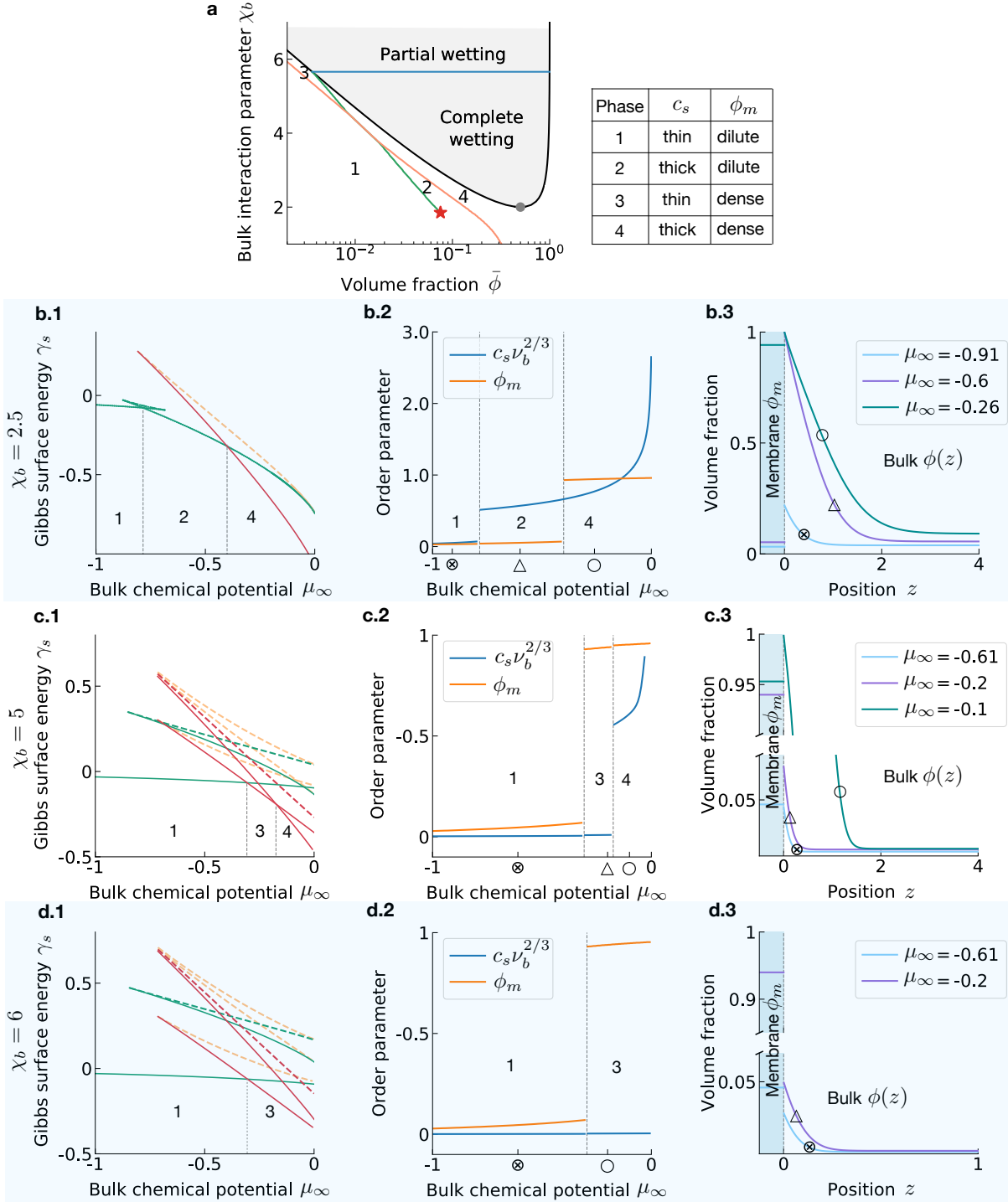


FIG. 5. **Binding to phase-separated membranes with attractive bulk-membrane coupling.** (a) Surface phase diagram showing multiple prewetting transition lines separating different surface states (see table). Parameter values are  $\chi_{bm} = -0.1$ ,  $\omega_m = -0.3$ . We consider three bulk interaction values  $\chi_b = 2.5, 5, 6$ . (b.1, c.1, d.1) The Gibbs surface free energy  $\gamma_s$  as a function of the chemical potential  $\mu_\infty$ . (b.2, c.2, d.2) Excess surface concentration  $c_s$  (Eq. (4)) and membrane area fraction  $\phi_m$ . (b.3, c.3, d.3) Bulk volume fraction profiles  $\phi(z)$  and  $\phi_m$ .

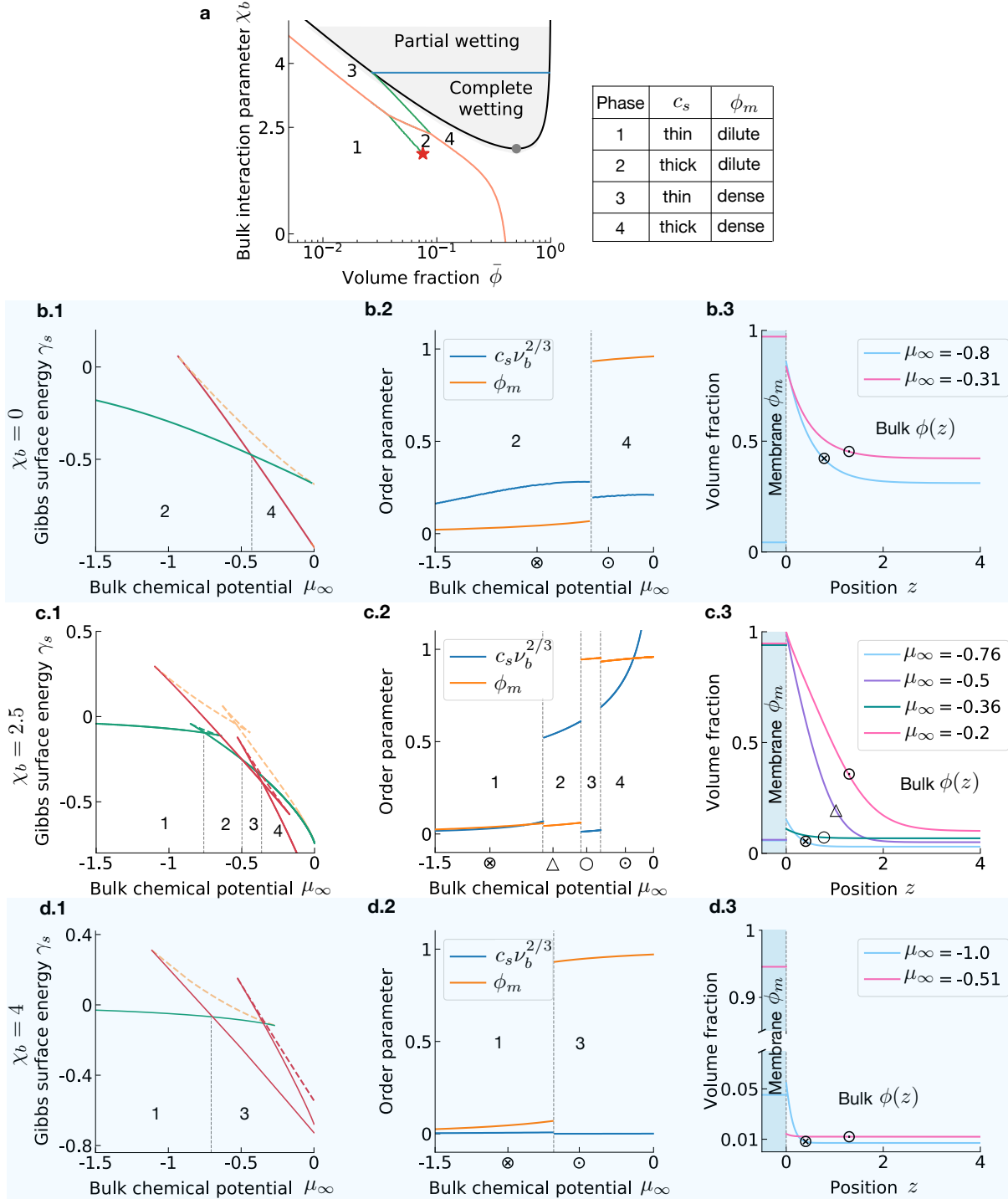


FIG. 6. **Binding to phase-separated membranes with repulsive bulk-membrane coupling.** (a) Surface phase diagram showing multiple prewetting transition lines separating different surface states (see table);  $\chi_{bm} = 0.3$  and  $\omega_m = -0.7$ . We consider three bulk interaction values  $\chi_b = 0, 2.5$ , and  $4$ . (b.1, c.1, d.1) The Gibbs surface free energy  $\gamma_s$  as a function of the chemical potential  $\mu_\infty$ . (b.2, c.2, d.2) Excess surface concentration  $c_s$  (Eq. (4)) and membrane area fraction  $\phi_m$ . (b.3, c.3, d.3) Bulk volume fraction profiles  $\phi(z)$  and  $\phi_m$ .

stable branches, which are connected by a locally unstable branch. To illustrate the Gibbs loop for prewetting transitions with membrane binding, we show the Gibbs surface energy  $\gamma_s$  as a function of the chemical potential of the reservoir,  $\mu_\infty$  (Fig. 5(b1,c1,d1) and 6(b1,c1,d1)). At the phase transitions, the Gibbs surface energy of the thermodynamic state exhibits a kink, while the locally stable (solid lines) and unstable (dashed lines) branches form the Gibbs loops. We find that the complexity of such Gibbs loops is different for different values of the bulk interaction  $\chi_b$ . For example, we find classical Gibbs loops where two locally stable branches and one unstable branch exists in a certain chemical potential range of  $\mu_\infty$  (Fig. 6(b1)). We also find cases where up to four locally stable surface states exists (Fig. 5(b1,c1,d1) and 6(c1,d1)). This structure of nested Gibbs loops suggest a complex dynamics towards equilibrium.

## 2. Correlated and anti-correlated jumps of surface order parameters

The coupling between membrane and bulk implies that in general both order parameters, the excess surface concentration  $c_s$  and the bound area fraction in membrane  $\phi_m$ , jump at the transition lines. The sign of each jump is determined by whether the coupling is attractive ( $\chi_{bm} < 0$ ) or repulsive ( $\chi_{bm} > 0$ ). Specifically, for attractive couplings, both order parameters jump upwards as the chemical potential  $\mu_\infty$  is increased, while for repulsive couplings, order parameters can show jumps in opposite directions.

For attractive bulk-membrane couplings ( $\chi_{bm} < 0$ ), and increasing chemical potential  $\mu_\infty$ , either  $c_s$  or  $\phi_m$  shows a pronounced jump upwards. This depends on the bulk interaction  $\chi_b$  (compare Fig. 5(b.2) for  $\chi_b = 2.5$  with Fig. 5(b.3) for  $\chi_b = 5$ ). For more attractive bulk interactions ( $\chi_b = 5$  versus  $\chi_b = 2.5$ ), molecules prefer binding to accumulating at the membrane surface. Thus, the order parameters for membrane binding  $\phi_m$  show the pronounced jump first as the chemical potential  $\mu_\infty$  is increased (c.2), while for less attractive bulk interactions, the excess surface concentration  $c_s$  makes the bigger jump first (b.2). To illustrate the different hierarchies of the order parameter jumps, we colorize the transition line according to a dominant  $c_s$  jump (green line) or a dominant  $\phi_m$  jump (orange line) in Fig. 5(a) and Fig. 6(a). Thus, for the case of attractive bulk-membrane coupling, the layer width of the profile  $\phi(z)$  as well as  $c_s$  increases for increasing  $\mu_\infty$  (Fig. 5(b.3,c.3, d.3)). In other words, the more molecules are in the bulk, the thicker the prewetted layer.

This behavior changes for the case of a repulsive bulk-membrane coupling ( $\chi_{bm} > 0$ ). In this case, at each transition, both order parameters jump into opposite directions. Such opposite jumps



can even cause a decrease in layer thickness of the profile  $\phi(z)$  (Fig. 6(c.3)). Similar to the case of attractive couplings, the jump heights and the number of jumps depend on the bulk interactions  $\chi_b$  (Fig. 6(b.2, c.2, d.2)).

### C. Wetting and prewetting with related bulk and surface interactions

In the last two sections we discussed wetting and prewetting for bulk interaction parameters  $\chi_b$  and coupling parameters between bulk and membrane  $\chi_{bm}$  that were varied independently from each other. However, if molecules bound to the membrane are the same as the molecules in the bulk, both parameters describe similar physical interactions and are therefore related. This relationship is specific to the system of interest and can depend on the membrane composition and the type of solvent and bulk molecule. To account for a relation between the interaction parameters  $\chi_b$  and  $\chi_{bm}$ , we consider for simplicity a linear relationship,

$$\chi_{bm} = -\alpha \chi_b, \quad (16)$$

where  $\alpha$  describes the correlation between both interaction parameters. Interactions among bulk molecules and interaction of bulk with membrane-bound molecules can have equal (correlated,  $\alpha > 0$ ) or opposite ( $\alpha < 0$ ) signs, which we refer to the correlated and anti-correlated case, respectively. A positive  $\alpha$  applies if interactions in the bulk are similar to interactions between bulk and bound molecules. A negative  $\alpha$  could for example correspond to a situation where the molecular domain mediating the interactions in the bulk  $\chi_b$  is also involved in binding to the surface and thus not accessible for interactions of bound molecules with bulk molecules  $\chi_{bm}$ . Here, the interactions among membrane-bound molecules  $\chi_m$  are kept constant.

In the following, we study the phase diagrams of prewetting and wetting for correlated and anti-correlated interaction parameters. Moreover, we keep the interactions  $\chi_m$  among membrane-bound molecule constant and distinguish between the cases with ( $\chi_m = 3$ ) and without ( $\chi_m = -4$ ) phase separation in the membrane. We show that either the wetting transition can be suppressed, while prewetted states can robustly occur below saturation.

#### 1. *Suppression of partial wetting*

We first discuss the case of membrane-bound molecules that do not phase-separate in the membrane (e.g.  $\chi_m = -4$ ). For correlated  $\chi_b$  and  $\chi_{bm}$  ( $\alpha > 0$ ), partially wetted states are suppressed and complete wetting always occurs in the supersaturated regime (Fig. 7a). In this case, there

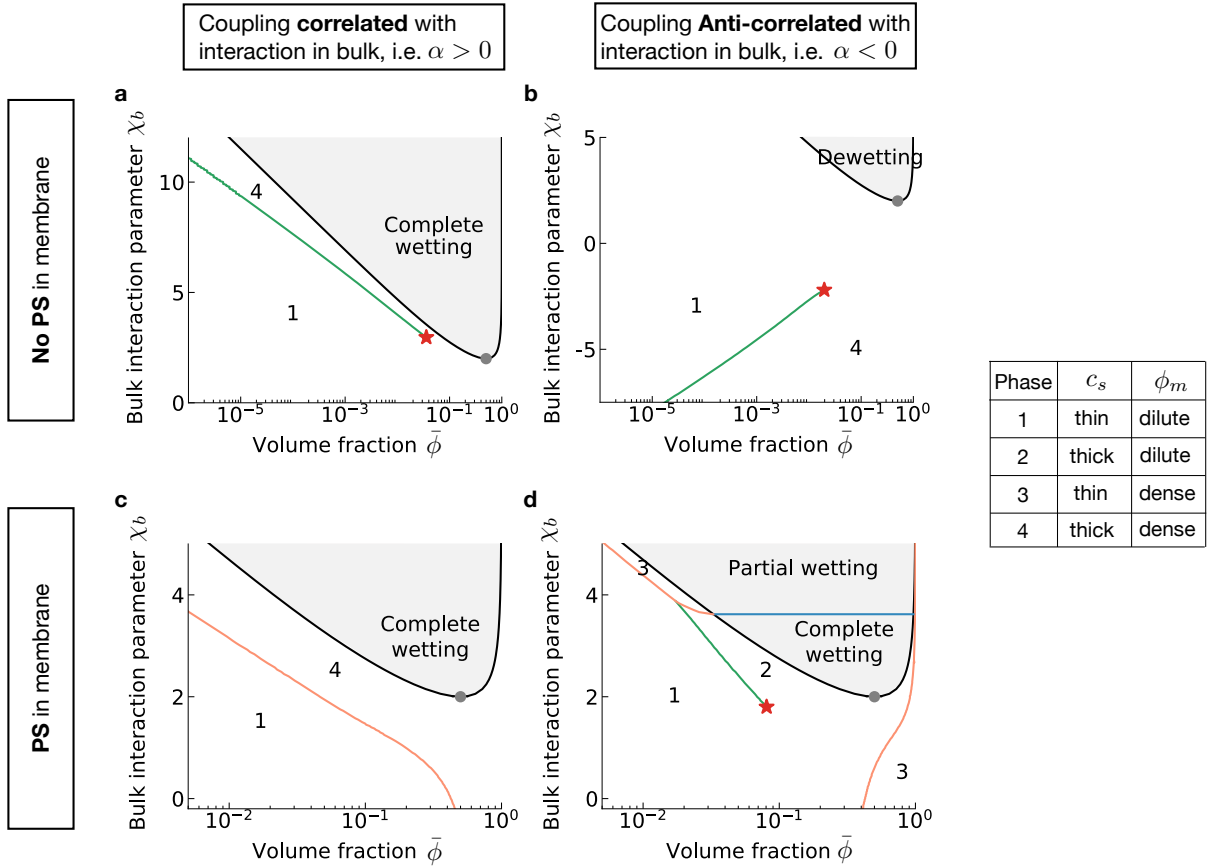


FIG. 7. **Surface phase diagram with interdependent interaction parameters  $\chi_{bm}$  and  $\chi_b$ .** The membrane-bound molecules cannot phase-separate in (a) and (b) ( $\chi_m = -4$ ), while they are able to phase-separate in (c) and (d) ( $\chi_m = 3$ ). In addition, we distinguish between bulk interactions  $\chi_b$  and membrane-bulk interactions  $\chi_{bm}$  of equal (correlated,  $\alpha > 0$ ) and opposite signs (anti-correlated,  $\alpha < 0$ ); see Eq. (16). Parameters: (a)  $\alpha = 0.4$ . (b)  $\alpha = -2.8$ . (c)  $\alpha = 0.5$ . (d)  $\alpha = -0.5$ .

is no wetting transition line and the prewetting line does not merge with the binodal. Moreover, the prewetting region where thick layers form enlarges for increasing bulk interaction parameter  $\chi_b$ . The reason for the homogeneous states (completely wetted, thick layer) being favored on the membrane surface is that larger  $\chi_b$  also implies more attractive bulk-membrane coupling ( $\alpha > 0$ ). For anti-correlated  $\chi_b$  and  $\chi_{bm}$  ( $\alpha < 0$ ), wetting can be completely suppressed for attractive bulk interactions ( $\chi_b > 0$ ); see Fig. 7b. In other words, within the supersaturated regime, there are no condensates at the membrane surface. However, prewetted states can form for repulsive interactions among bulk molecules ( $\chi_b < 0$ ). This case represents an ideal scenario to either prevent bulk condensates from interacting with surfaces or to enable prewetted condensates at surface without the capability of the bulk to form condensates.

Now we discuss the case where membrane-bound molecules can phase-separate in the membrane (e.g.  $\chi_m = 4$ ). If  $\chi_b$  and  $\chi_{bm}$  are correlated ( $\alpha > 0$ ), complete wetting is favored over partial wetting in the supersaturated regime (Fig. 7c), similar to the case without phase separation in the membrane (Fig. 7a). Also, the domain of prewetted states broadens as the bulk interaction parameters get more attractive. The only qualitative difference to the case without phase separation in the membrane is that there is no critical point of prewetting (Fig. 7c). The reason is that though both, bulk interactions (negative  $\chi_b$ ) and membrane-bulk interactions get more repulsive, the ability to phase-separate in the membrane can still enable thick layers at the membrane surface. For anti-correlated  $\chi_b$  and  $\chi_{bm}$  ( $\alpha < 0$ ) in the presence of phase separation in the membrane (Fig. 7d), the resulting phase diagram combine features of previously discussed diagrams. For example, due to anti-correlated interaction parameters, the wetting transition is maintained and the prewetting line merges with the binodal. Interestingly, the prewetting line curves upwards opposite to classical prewetting phase diagrams. Furthermore, for strongly attractive bulk interactions (large  $\chi_b$ ) prewetting can even occur at conditions below the bulk critical point mediated by phase separation in the membrane. Finally, the membrane phase transition in the absence of bulk interactions (e.g.  $\chi_b = 0$ ) is now disconnected from the prewetting lines but converges to the binodal of the dense phase (Fig. 7d).

## 2. *Antagonism between membrane-bound and prewetted layers*

In classical wetting and prewetting (Fig. 3a), the profile of a thick layer curves upwards when approaching the surface due to attractive interactions between bulk and surface ( $\omega_b < 0$ ). In the presence of membrane binding this leads to a high volume fraction  $\phi_m$  in the membrane for correlated interaction parameters ( $\alpha > 0$ ). This situation can fundamentally change when membrane binding and prewetting are antagonistic due to anti-correlated interaction parameters ( $\alpha < 0$ ). As a result of this anti-correlation, we can distinguish between two types of antagonistic cases. First, a thick prewetting layer near the surface can induce detachment of molecules from the surface (purple lines in Fig. 9c). Molecules cannot bind to the surface and thus the surface is effectively attractive. Second, molecules bind to the membrane surface which thereby becomes repulsive for bulk molecules. No prewetting layer forms and the concentration profile even curves downward when approaching the surface (see Fig. 9c).

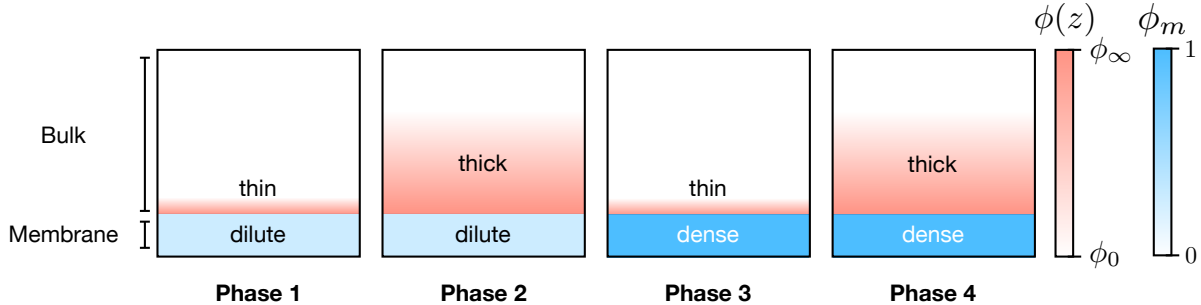


FIG. 8. **Overview of surface states for systems where molecules can bind to a membrane surface.** We find four surface states which are each characterized by a pair of order parameters, i.e., the volume fraction of molecules bound to the surface,  $\phi_m$ , and the excess surface concentration,  $c_s$  (Eq. (4)). Depending on the interactions between bulk and surface, the membrane can be either dilute (light blue, low  $\phi_m$ ) or dense (dark blue, high  $\phi_m$ ), and the bulk layer can be either thin (low  $c_s$ ) or thick (high  $c_s$ ). The shades of red show the bulk profile  $\phi(z)$  which ranges between the bulk volume fraction  $\phi_\infty$  and the volume fraction at the membrane surface  $\phi|_0$  (see colorbar).

#### IV. DISCUSSION

Due to the significance of both binding processes and bulk condensation in living cells we study how membrane binding affects surface phase transitions. To approach this question, we derive the thermodynamic theory of wetting and prewetting in the presence of binding at thermodynamic equilibrium. Our theory goes beyond the classical thermodynamics of surface phase transitions by introducing new surface states. Recently, related questions were addressed using Monte-Carlo simulations of a ternary lattice model for mobile tethers that are confined in a membrane and that can bind bulk molecules [33]. This work focuses on the role of three phase coexistence in the membrane.

In our theory we focus on a binary mixture in the bulk that interacts with a surface layer bound to a flat and rigid membrane. Our thermodynamic theory reveals that membrane binding can lead to a variety of new thermodynamic wetting and prewetting states with unexpectedly rich surface phase diagrams. Such wetted and prewetted states are described by a pair of order parameters, i.e., the fraction of bound molecules in a single surface layer and the excess surface concentration of the condensates adjacent to the surface (see Fig. 8). Interestingly, we find cases where surface phase transitions occur under conditions where the bulk cannot phase-separate at any concentration. More generally, a layer of bound molecules on the membrane effectively modifies the properties of the surface which can for example lead to a shift of the prewetting line to low concentrations.

Finally, surface binding affects the wetting transition and the contact angle of bulk droplets that wet the surface.

Our findings suggest that the binding of molecules provides a versatile mechanism to control the position of wetted droplets under supersaturated conditions. In recent years, a growing number of intra-cellular condensates were shown to adhere to membrane-bound organelles or the intra-cellular surfaces [2, 7, 8, 23, 34]. Moreover, many of such condensates are suggested to act as scaffolds for biochemical processes [35, 36]. Specific binding receptors at the membrane surface can control the position of such wetted droplets and thereby spatially control biological processes occurring inside droplets.

We also find that binding alters the prewetting behavior below saturation. While the classical prewetting transition line is very close to the saturation concentration ([20, 37]; see also Fig. 3(a)), the transition line shifts to lower values for systems where molecules can bind to membrane surfaces. Interestingly, the actual physiological concentrations of many membrane-binding proteins in living cells (typically  $(10 - 100)nM$  [21–23, 38]) are far below their saturation concentrations (typically  $(1 - 10)\mu M$  [23, 34]). Further research is required to scrutinize whether the low physiological concentrations of membrane-binding proteins serve the purpose to form prewetted condensates on intracellular surfaces rather than droplets in the bulk.

Returning to Pauli’s famous quote, surfaces in biological systems were probably not invented by the devil. Rather, membranes and surfaces have an essential functional role for living cells. This essential role is reflected in a plethora of biological processes ranging from cell division to intra- and extra-cellular transport. Binding to such surfaces together with surface phase transitions gives rise to a new level of complexity that is exemplified in the rich variety of phases and variability of phase diagrams revealed by our work. This suggests that this additional complexity could play a key role in cell biological processes. We expect that this complexity is further extended when binding processes are maintained away from thermodynamic equilibrium, which is the case in living cells. In biological systems, ATP-driven cycles of kinase and phosphatase can alter binding equilibria. Future research will clarify how such active binding processes modify the properties of wetted and prewetted states out of equilibrium.

## ACKNOWLEDGMENTS

We thank S. Liese, J. Bauermann, L. Hubatsch, S. Bo, S. Laha, T. Harmon, I. LuValle-Burke, and D. Sun for insightful discussions and S. Liese for helpful feedback on the manuscript. G.

Bartolucci, A. Honigmann, and C. Weber acknowledge the SPP 2191 “Molecular Mechanisms of Functional Phase Separation” of the German Science Foundation for financial support and for providing an excellent collaborative environment.

---

- [1] B. Jamtveit and P. Meakin. Growth, dissolution and geosystems. *Springer Netherlands*, page 291, 1999.
- [2] Clifford P. Brangwynne, Christian R. Eckmann, David S. Courson, Agata Rybarska, Carsten Hoegel, Jöbin Gharakhani, Frank Jülicher, and Anthony A. Hyman. Germline p granules are liquid droplets that localize by controlled dissolution/condensation. *Science*, 324(5935):1729–1732, 2009.
- [3] Anthony A. Hyman, Christoph A. Weber, and Frank Jülicher. Liquid-liquid phase separation in biology. *Annual Review of Cell and Developmental Biology*, 30(1):39–58, 2014.
- [4] Salman F. Banani, Hyun O. Lee, Anthony A. Hyman, and Michael K. Rosen. Biomolecular condensates: organizers of cellular biochemistry. *Nature Reviews Molecular Cell Biology*, 18, 2017.
- [5] Clifford P. Brangwynne, Timothy J. Mitchison, and Hyman Anthony A. Active liquid-like behavior of nucleoli determines their size and shape in xenopus laevis oocytes. *Proceedings of the National Academy of Sciences*, 108(11):4334–4339, 2011.
- [6] Marina Feric, Nilesh Vaidya, Tyler S. Harmon, Diana M. Mitrea, Lian Zhu, Tiffany M. Richardson, Richard W. Kriwacki, Rohit V. Pappu, and Clifford P. Brangwynne. Coexisting liquid phases underlie nucleolar subcompartments. *Cell*, 165(7):1686–1697, 2016.
- [7] Joseph G. Gall, Michel Bellini, Zheng’an Wu, and Christine Murphy. Assembly of the nuclear transcription and processing machinery: Cajal bodies (coiled bodies) and transcriptosomes. *Molecular Biology of the Cell*, 10(12):4385–4402, 1999.
- [8] Jaime Agudo-Canalejo, Sebastian W. Schultz, Haruka Chino, Simona M. Migliano, Chieko Saito, Ikuko Koyama-Honda, Harald Stenmark, Andreas Brech, Alexander I. May, Noboru Mizushima, and Roland L. Knorr. Wetting regulates autophagy of phase-separated compartments and the cytosol. *Nature*, 591:142–146, 2021.
- [9] John W. Cahn. Critical point wetting. *The Journal of Chemical Physics*, 66(8):3667–3672, 1977.
- [10] Hisao Nakanishi and Michael E. Fisher. Multicriticality of wetting, prewetting, and surface transitions. *Phys. Rev. Lett.*, 49:1565–1568, Nov 1982.
- [11] P. G. de Gennes. Wetting: statics and dynamics. *Rev. Mod. Phys.*, 57:827–863, Jul 1985.
- [12] Hans Werner Diehl and Siegfried Dietrich. *Static and dynamic critical behavior at surfaces*, pages 39–52. Springer Berlin Heidelberg, Berlin, Heidelberg, 1985.
- [13] Martin P. Gelfand and Reinhard Lipowsky. Wetting on cylinders and spheres. *Phys. Rev. B*, 36:8725–8735, Dec 1987.
- [14] H. W. Diehl. The theory of boundary critical phenomena. *International Journal of Modern Physics B*, 11(30):3503–3523, Dec 1997.

- [15] Daniel Bonn, Jens Eggers, Joseph Indekeu, Jacques Meunier, and Etienne Rolley. Wetting and spreading. *Rev. Mod. Phys.*, 81:739–805, May 2009.
- [16] Reinhard Lipowsky. Response of membranes and vesicles to capillary forces arising from aqueous two-phase systems and water-in-water droplets. *The Journal of Physical Chemistry B*, 122(13):3572–3586, 2018.
- [17] M. Napiórkowski, L. Schimmele, and S. Dietrich. Wetting transitions on soft substrates. *EPL (Europhysics Letters)*, 129(1):16002, Feb 2020.
- [18] J.E. Rutledge and P. Taborek. Prewetting phase diagram of  $^4\text{He}$  on cesium. *Phys. Rev. Lett.*, 69:937, 1992.
- [19] S. Chandavarkar, R. M. Geertman, and W. H. de Jeu. Observation of a prewetting transition during surface melting of caprolactam. *Phys. Rev. Lett.*, 69:2384–2387, 1992.
- [20] H. Kellay, D. Bonn, and J. Meunier. Prewetting in a binary liquid mixture. *Phys. Rev. Lett.*, 71:2607, 1993.
- [21] Sudeep Banjade and Michael K Rosen. Phase transitions of multivalent proteins can promote clustering of membrane receptors. *Elife*, 3:e04123, 2014.
- [22] Xiaolei Su, Jonathon A Ditlev, Enfu Hui, Wenmin Xing, Sudeep Banjade, Julia Okrut, David S King, Jack Taunton, Michael K Rosen, and Ronald D Vale. Phase separation of signaling molecules promotes t cell receptor signal transduction. *Science*, 352(6285):595–599, 2016.
- [23] Oliver Beutel, Riccardo Maraschini, Karina Pombo-García, Cécilie Martin-Lemaitre, and Alf Honigmann. Phase separation of zonula occludens proteins drives formation of tight junctions. *Cell*, 179(4):923–936.e11, 2019.
- [24] Martin Loose, Elisabeth Fischer-Friedrich, Jonas Ries<sup>1</sup>, Karsten Kruse, and Petra Schwille. Spatial regulators for bacterial cell division self-organize into surface waves in vitro. *Science*, 320:789–792, 2008.
- [25] Jacob Halatek and Erwin Frey. Highly canalized mind transfer and mine sequestration explain the origin of robust mincde-protein dynamics. *Cell Reports*, 1(6):741–752, 2012.
- [26] Beatrice Ramm, Tamara Heermann, and Petra Schwille. The e. coli mincde system in the regulation of protein patterns and gradients. *Cellular and Molecular Life Sciences*, 76:4245–4273, 2019.
- [27] Cornelia Schwayer, Shayan Shamipour, Kornelija Pranjic-Ferscha, Alexandra Schauer, Maria Balda, Masazumi Tada, Karl Matter, and Carl-Philipp Heisenberg. Mechanosensation of tight junctions depends on zo-1 phase separation and flow. *Cell*, 179(4):937 – 952.e18, 2019.
- [28] Jaime Agudo-Canalejo, Sebastian W Schultz, Haruka Chino, Simona M Migliano, Chieko Saito, Ikuko Koyama-Honda, Harald Stenmark, Andreas Brech, Alexander I May, Noboru Mizushima, et al. Wetting regulates autophagy of phase-separated compartments and the cytosol. *Nature*, 591(7848):142–146, 2021.
- [29] Thomas Quail, Stefan Golfier, Maria Elsner, Keisuke Ishihara, Frank Jülicher, and Jan Brugués. Capillary forces drive pioneer transcription factor-mediated dna condensation. *bioRxiv*, 2020.

- [30] Jose A. Morin, Sina Wittmann, Sandeep Choubey, Adam Klosin, Stefan Golfier, Anthony A. Hyman, Frank Jülicher, and Stephan W. Grill. Surface condensation of a pioneer transcription factor on dna. *bioRxiv*, 2020.
- [31] Wilton T Snead and Amy S Gladfelter. The control centers of biomolecular phase separation: how membrane surfaces, ptms, and active processes regulate condensation. *Molecular cell*, 76(2):295–305, 2019.
- [32] Pritam Kumar Jana and Bortolo Matteo Mognetti. Surface-triggered cascade reactions between dna linkers direct the self-assembly of colloidal crystals of controllable thickness. *Nanoscale*, 2019.
- [33] Mason Rouches, Sarah Veatch, and Benjamin Machta. Surface densities prewet a near-critical membrane. *bioRxiv*, 2021.
- [34] Ziheng Liu, Ying Yang, Aihong Gu, Jiawen Xu, Ying Mao, Weiguo Hu Haojie Lu, Qun-Ying Lei, Zhouhua Li, Mingjie Zhang, Yu Cai, and Wenyu Wen. Par complex cluster formation mediated by phase separation. *Nature Communications*, 11, 2020.
- [35] Steven Boeynaems, Simon Alberti, Nicolas L Fawzi, Tanja Mittag, Magdalini Polymenidou, Frederic Rousseau, Joost Schymkowitz, James Shorter, Benjamin Wolozin, Ludo Van Den Bosch, et al. Protein phase separation: a new phase in cell biology. *Trends in cell biology*, 28(6):420–435, 2018.
- [36] Simon Alberti, Amy Gladfelter, and Tanja Mittag. Considerations and challenges in studying liquid-liquid phase separation and biomolecular condensates. *Cell*, 176(3):419–434, 2019.
- [37] James W. Schmidt and Michael R. Moldover. First-order wetting transition at a liquid-vapor interface. *Journal of Chemical Physics*, 79, 1983.
- [38] Nathan W. Goehring, Philipp Khuc Trong, Justin S. Bois, Debanjan Chowdhury, Ernesto M. Nicola, Anthony A. Hyman, and Stephan W. Grill. Polarization of par proteins by advective triggering of a pattern-forming system. *Science*, 334:1137–1141, 2011.



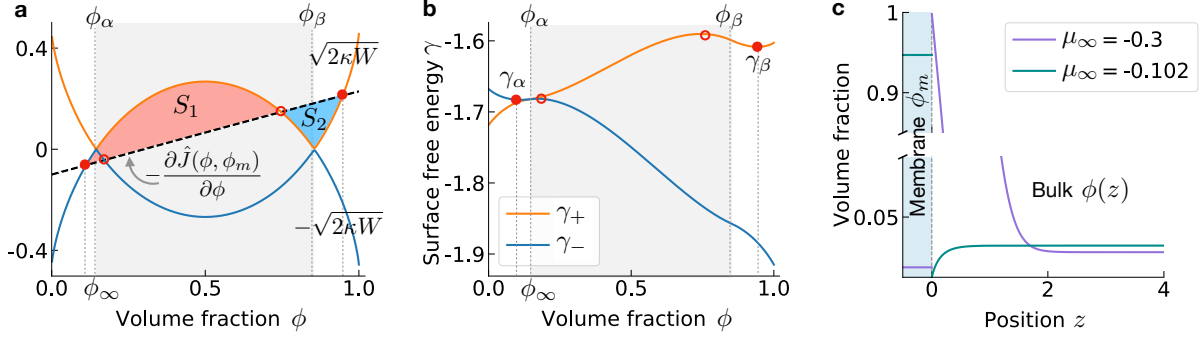


FIG. 9. **Graphical construction for wetting with both solution branches in Eq. (A5).** (a)  $-\partial\hat{J}(\phi, \phi_m)/\partial\phi$  (dashed line) can intersect with both branches  $\sqrt{2\kappa W}$  (solid orange line) and  $-\sqrt{2\kappa W}$  (solid blue line). The intersection points correspond to two local minima (solid red points) and two local maxima (empty red points). (b) We create a free energy landscape  $\gamma$  by varying the surface volume fraction while maintaining one of the equilibrium conditions Eq. (10c). For each branch in (a), we calculate the surface free energy  $\gamma_+ = \int_{\phi_\infty}^{\phi} d\phi' \left[ \sqrt{2\kappa W(\phi')} + \frac{\partial\hat{J}}{\partial\phi'} \right] + \hat{J}(\phi_\infty, \phi_m)$  (orange line) and  $\gamma_- = \int_{\phi_\infty}^{\phi} d\phi' \left[ -\sqrt{2\kappa W(\phi')} + \frac{\partial\hat{J}}{\partial\phi'} \right] + \hat{J}(\phi_\infty, \phi_m)$  (blue line). The stability of the solutions (red solid and empty symbols) is determined by the local curvature of Gibbs surface free energy. The gray shaded area represents the demixed regime where the bulk can phase separate into a dilute phase with volume fraction  $\phi_\alpha$  and a dense phase where the volume fraction is  $\phi_\beta$ . (c) Two examples of concentration profile: one with convex shape near by the surface (purple solid line), while another with concave meniscus (green solid line).

### Appendix A: Graphical construction for surface phase transitions with membrane binding

Eqs. (9) are one differential equation of second order for the bulk volume fraction  $\phi(z)$  coupled to three algebraic equations at the membrane boundary and at  $z \rightarrow \infty$ . In this section, we integrate once, leading to a differential equation of first order coupled to two algebraic equations. The resulting set of equations can then be solved by a graphical construction which is similar to Ref. [9].

After multiplying Eq. (9a) by  $(\partial\phi/\partial z)$  on both sides, one obtains

$$\frac{\partial f_b}{\partial z} - \frac{1}{\nu_b} \mu_\infty \frac{\partial\phi}{\partial z} - \frac{\partial}{\partial z} \left( \frac{\kappa}{2} (\partial_z \phi)^2 \right) = 0. \quad (\text{A1})$$

Integrating this equation over the bulk,

$$\int_z^\infty dz' \left[ \frac{\partial f_b}{\partial z'} - \frac{1}{\nu_b} \mu_\infty \frac{\partial\phi}{\partial z'} - \frac{\partial}{\partial z'} \left( \frac{\kappa}{2} (\partial_{z'} \phi)^2 \right) \right] = 0, \quad (\text{A2})$$

and utilising boundary conditions  $\partial_z \phi|_{\infty} = 0$  (Eq. (9b)), and  $\phi(\infty) = \phi_{\infty}$ , we obtain

$$0 = f_b(\phi(z)) - f_b(\phi_{\infty}) - \mu_{\infty} \left( \frac{1}{\nu_b} \phi(z) - \frac{1}{\nu_b} \phi_{\infty} \right) - \frac{\kappa}{2} (\partial_z \phi)^2. \quad (\text{A3})$$

Using the definition of  $W(\phi)$  (Eq. (10d)), Eq. (A3) can be written as

$$|\partial_z \phi|^2 = \frac{2}{\kappa} W(\phi), \quad (\text{A4})$$

leading to two solution branches (orange and blue lines in Fig. 9):

$$\partial_z \phi = \pm \sqrt{\frac{2}{\kappa} W(\phi)}. \quad (\text{A5})$$

Finally, substituting these two relations into Eq. (9c), we obtain Eq. (10b). Please note that since we have already used Eq. (9b) in the derivation above, we are left with two algebraic equations and one ODE of first order (see Eqs. (10)). These equations can be solved via a graphical construction to obtain the surface volume fraction  $\phi|_0$  and membrane area fraction  $\phi_m$  at thermodynamic equilibrium; see Fig. 9 for an illustration in the presence of the two solution branches (Eq. (A5)).

Numerical solutions of Eqs. (10) may suffer from the fact that the bulk chemical potential  $\mu_b = \partial f_b / \partial \phi$  is singular for  $\phi = 1$ . To avoid numerical problems related to this singularity, we can add a term of the form  $-\epsilon(1 - \phi) \ln(1 - \phi)$  to the coupling free energy  $J$  such that  $-\partial J / \partial \phi|_0$  can always intersect with  $\sqrt{2\kappa W}$  in the limit  $\phi \rightarrow 1$ . We note that  $\epsilon = 10^{-3}$  is a very small number to ensure that the thermodynamic states are hardly affected.

## Appendix B: Condition of critical prewetting

In this section, we derive the condition for prewetting critical points with membrane binding. At the prewetting critical point, the Gibbs surface potential  $\gamma_s(\phi|_0)$  given in Eq. (11) has a zero curvature with respect to  $\phi|_0$ ,

$$\frac{\kappa W'(\phi|_0)}{\sqrt{2\kappa W(\phi|_0)}} \pm \frac{\partial^2 J(\phi, \phi_m)}{\partial \phi^2} \Big|_0 \pm \frac{\partial^2 J(\phi, \phi_m)}{\partial \phi \partial \phi_m} \frac{\partial \phi_m}{\partial \phi} \Big|_0 = 0, \quad (\text{B1})$$

where  $\partial \phi_m / \partial \phi|_0$  can be obtained from the derivative of Eq. (10c):

$$\frac{\partial^2 f_m}{\partial \phi_m^2} \frac{\partial \phi_m}{\partial \phi} \Big|_0 + \frac{\partial^2 J(\phi, \phi_m)}{\partial \phi_m^2} \frac{\partial \phi_m}{\partial \phi} \Big|_0 + \frac{\partial^2 J(\phi, \phi_m)}{\partial \phi_m \partial \phi} \Big|_0 = 0. \quad (\text{B2})$$

Substituting  $J(\phi, \phi_m)$  given in Eq. (15c) and  $f_m$  given in Eq. (15), we obtain

$$\frac{\partial \phi_m}{\partial \phi} \Big|_0 = \chi_{bm} \frac{\phi_m(1 - \phi_m)}{(1 - 2\chi_m \phi_m(1 - \phi_m))}. \quad (\text{B3})$$

Combining Eq. (B1) with Eq. (B3), we find the condition for prewetting critical point,

$$\sqrt{\frac{\kappa}{2W(\phi)}} \frac{\tilde{\nu}}{\nu_b} \left[ \ln \phi - n_b \ln(1 - \phi) + n_b \chi_b (1 - 2\phi) - \frac{\mu_\infty}{k_B T} \right]_0 \pm \left[ \chi_{bb} + \chi_{bm}^2 \frac{\phi_m(1 - \phi_m)}{(1 - 2\chi_m \phi_m(1 - \phi_m))} \right] = 0, \quad (\text{B4})$$

where  $W(\phi)$  is defined in Eq. (10d).